

Chapter 9

Molecular Electronics

Subhasis Ghosh

Abstract Molecular electronics aim to create a functional electronic device using single or small assembly of molecules. It is believed that molecular electronics, not only will meet the increasing demand of more speed and more storage, but also provide a test bed to investigate mesoscopic transport phenomena and different properties at molecular level. Though there are several advantages in adopting single molecule as the active element in nanodevices, but contacting molecule with macroscopic contact in a circuit still remains a major challenge, as the conventional lithography-based contacting techniques cannot form metal contacts to a single molecule. Moreover, the absence of suitable imaging techniques at subnanometer level to look into single metal-molecule junction makes it even harder challenge. In last decade, several novel contacting techniques using nanolithography have been developed. However, the evidence that a molecule has been docked and contacted between two metal electrodes successfully can only be provided by measuring the current transport through the junctions. Out of the different mesoscopic devices in the length scale of 1–3 nm, it has been emphasized that molecular devices based on electrical break junction will be most suitable for electrical characterization with a prospect to use them in future circuits based on single molecule-based nanodevices. These investigations on the electrical transport through single or small assembly of molecules should be extremely useful for understanding quantum transport processes through the molecule, the device fabrication processes at nanoscale, and the roadmap for future nanoelectronics are essential for overcoming the “red brick wall” of Si-based microelectronics.

S. Ghosh (✉)

School of Physical Sciences, Jawaharlal Nehru University, New Delhi, India
e-mail: subhasis@mail.jnu.ac.in; subhasis.ghosh.jnu@gmail.com

S. Ghosh

Department of Physics, Shiv Nadar University, Greater Noida, India

© Springer Nature Singapore Pte Ltd. 2018

Z.H. Khan (ed.), *Nanomaterials and Their Applications*,

Advanced Structured Materials 84, https://doi.org/10.1007/978-981-10-6214-8_9

9.1 Introduction

The number of transistors in an integrated circuit grows exponentially, approximately doubling every two years following *Moore's law* [1]. The ever-increasing demand of the number of components requires scaling down feature size. This scaling down cannot be continued without reaching a classical or semi-classical limit, and eventually being dominated by quantum mechanical effects. Though *where-is-the-limit* is the subject of intense academic debate, but transistor with gate length less than 10 nm has been demonstrated and eventually incorporated in modern microchip. In addition to reduction in source to drain distance, the demand for ever-increasing switching speed has led to reduction of thickness of the gate oxides from 100 nm down to 1–2 nm, which is potentially detrimental for uncontrolled surface roughness and unwanted charge carriers tunneling. These uncontrolled and unwanted effects due to miniaturization of electronic devices lead to extensive research activities to develop nanodevices. One of the ways could be the use of single molecule-based electronic nanodevice and eventually electronic circuits. Molecule is the smallest conductor of electricity and arguably should be most preferred choice for active component in nanodevice. Molecule-based system should be naturally fault tolerant as there cannot be defect in single molecule, and molecules can be produced reproducibly in large numbers by chemical reactions which open up the almost infinite possibilities, in particular, in organic systems. Moreover, new functionalities or existing functionalities at a simpler process level can be provided by virtue of self-organization capabilities of molecules.

Aviram and Ratner [2] first proposed the use of single molecule as active electronic devices in 1974. They proposed that an organic molecule with built-in donor–acceptor moieties separated by a tunnel barrier could act as a rectifying diode. It took more than 20 years to realize organic molecule-based rectifying diode [3]. Absence of contacting technology to nanosystems was the biggest hindrance in achieving single molecule-based devices. After this discovery, an enormous amount of experimental results were presented using different novel contacting techniques [4–7]. But, during last decade, most of the achievement is more or less limited to *proof-of-concept*, because the reproducibility at nanometer scale appears to be extremely difficult challenge to overcome. Recently, several contacting techniques have shown promising results [4–7], which have shown reproducible results in organic molecule-based devices.

9.2 What Is Molecular Electronics?

As mentioned before, according to Moore's law, to achieve desired miniaturizing in near future, it will require to position atom by atom reproducibly and controllably. However, the technology required for this has not been realized yet, whereas it has been realized that it may be possible to position molecule by molecule to achieve

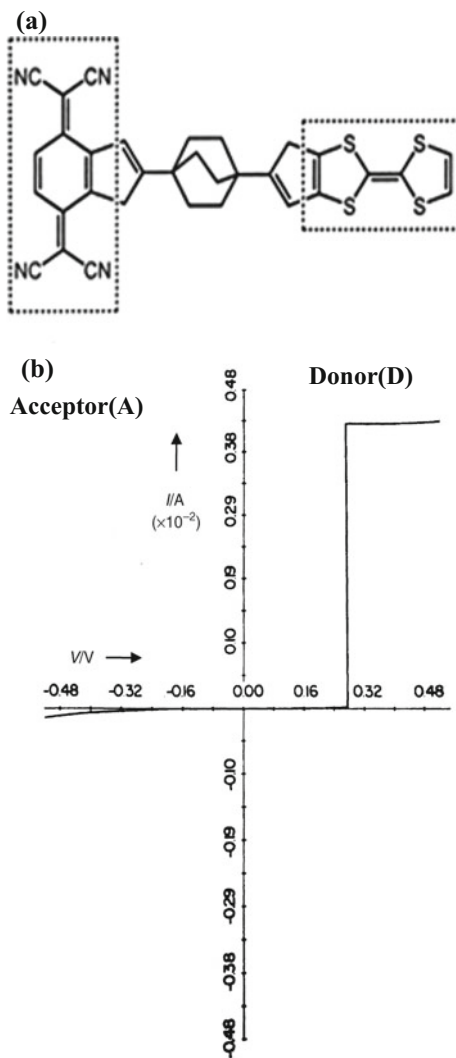
desired functionalities in electronic nanodevices. The field *molecular electronics* deals with all the issues related in realizing single or small assembly of molecules-based nanodevice that would perform all linear and nonlinear functionalities deemed for electronic devices. Initially, molecular electronics are defined as technologies utilizing only single molecules; however, this definition has been broadened by including electronic devices utilizing single molecular properties in small assemble of molecules, but differentiating from the field of electronics which utilized the properties of molecular solids, known as organic electronics. Essentially, molecular electronics is to be entirely based on molecule-based nanodevices deemed to break the technological bottleneck posed by Moore's law.

The simplest device is supposed to conceive a switch which should perform similar way as in Si-based devices, i.e., with well-defined addressable ON and OFF states and remaining in the state that it is placed until its state is changed by an external trigger. The addressability of molecular switch is not an issue in case of single molecule-based devices, but an area of major concern in devices which are based on assembling of molecules due to uncertainty in the position of molecule on a surface on which a particular configuration of molecules is required for certain functionalities. Another concern is the chemical stability of molecule under a wide variety of conditions. However, the biggest challenge is how to make a molecule connect with other molecules at nanoscale, as well as macroscale, extremely important for wiring up the molecules required for molecular circuit.

9.3 First-Generation Molecular Devices

The first-generation of molecular devices was proposed by Aviram and Ratner [2], based on an organic molecule with both donor and acceptor species, expected to show rectifying behavior analogous to conventional *p-n* junction. The proposed molecule composed of tetrathiafulvalene, a donor moiety connected by a methylene bridge to tetracyanoquinodimethane, an acceptor moiety, shown in Fig. 9.1. Metzger et al. [3] have successfully demonstrated rectification in Aviram–Ratner diode based on Langmuir Blodgett (LB) films of μ -(*n*-hexadecyl) quinolinium tricyanoquinodimethanide sandwiched between metal electrodes and observed rectification behavior. In this two terminal device, LB films of μ -(*n*-hexadecyl) quinolinium tricyanoquinodimethanide were deposited on aluminum (Al)-coated quartz or Silicon. Al layer evaporated on the LB films was for top contact. Figure 9.2 shows the current–voltage (*I–V*) characteristics for two devices. First device which showed a rectification ratio of 40 was based on single monolayer sandwiched between two Al electrodes. Second device was based on four monolayers to enhance the stability, but the rectification was reduced to 10. In the second type of devices, current was increased by three orders of magnitude most probably due to interface states between monolayers. Since the successful demonstration of unimolecular diode, there are several efforts [4, 5] to achieve higher rectification ratio in new molecular system. Wei et al. [8] have shown a rectification ratio of 10^3

Fig. 9.1 **a** Molecule proposed by Aviram and Ratner composed of donor (D) moiety tetrathiafulvalene connected by a methylene bridge (σ) to an acceptor (A) moiety, tetracyanoquinodimethane, **b** theoretically calculated I - V characteristics of metal/molecule/metal structure with the proposed molecule. Reprinted with permission from Ref. [2] Copyright (1974) Elsevier



in devices based on carbon nanotube asymmetrically functionalized with donor and acceptor moieties. Undoubtedly, these results help in progress of molecular electronics, but exact mechanism which is extremely important for further progress responsible for the rectification is still under intense debate.

As shown in Fig. 9.1, the molecule with an electron-rich moiety, i.e., tetrathiafulvalene (TTF) as donor (D) an electron-poor moiety, i.e., tetracyanoquinodimethane (TCNQ) as acceptor (A) linked by a covalent triple-methylene bridge as insulator (σ), generalized as D- σ -A molecule is sandwiched between two metallic

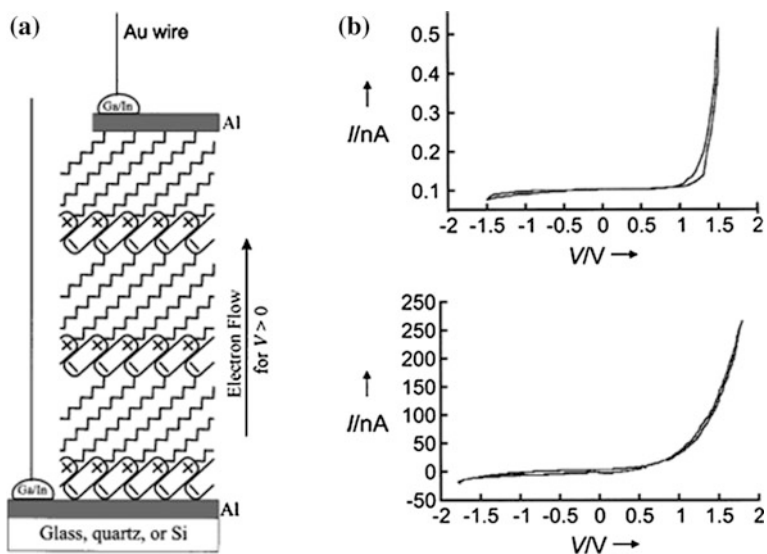


Fig. 9.2 **a** Schematic representation of the LB films structure of molecule μ -(*n*-hexadecyl)quinolinium tricyanoquinodimethanide on aluminum-coated Si or quartz. Either one or four monolayer of the molecule has been deposited. **b** I - V characteristics of two different devices. Al/1 LB monolayer/Al Ga/In eutectic and Al/4 LB monolayer/Al Ga/In eutectic. Reprinted with permission from Ref. [3] Copyright (1997) American Chemical Society

electrodes with two interfaces metal-D and metal-A. D and A regions of the molecular rectifiers are equivalent to n and p regions, respectively, in inorganic metallurgical p - n junction diode. However, D- σ -A molecular rectifier though appears to be a simple device, but is much more complex systems than inorganic p - n junctions. High and inhomogeneous electric fields resulted from the molecular dipoles in the monolayer, the screening induced by the molecules and the metallic electrodes, effect of high electric field on the electronic structure of molecules make these devices complex and require self-consistent quantum mechanical treatment for theoretical simulation. *ab initio* calculations have shown [9] that the direction of current flow in forward bias depends not only on the position of molecular level relative to the Fermi levels of the metal electrodes, but also on the bias-induced shift of the molecular levels resulting reverse rectification in opposite direction and may be responsible poor low rectification ratio generally observed in the these devices. It has been [10, 11] shown that any asymmetric coupling of the molecules with the electrodes or any asymmetry in the molecule could result in asymmetric I - V characteristics and rectification. Based on experimental observation, three different mechanisms by Aviram-Ratner (AR) [2], Kornilovitch-Bratkovsky-Williams (KBW) [12] and Datta-Paulsson (DP) [13] have been proposed to explain the rectification behaviors of molecular rectifier. These models are summarized in Fig. 9.3 [14] and described below.

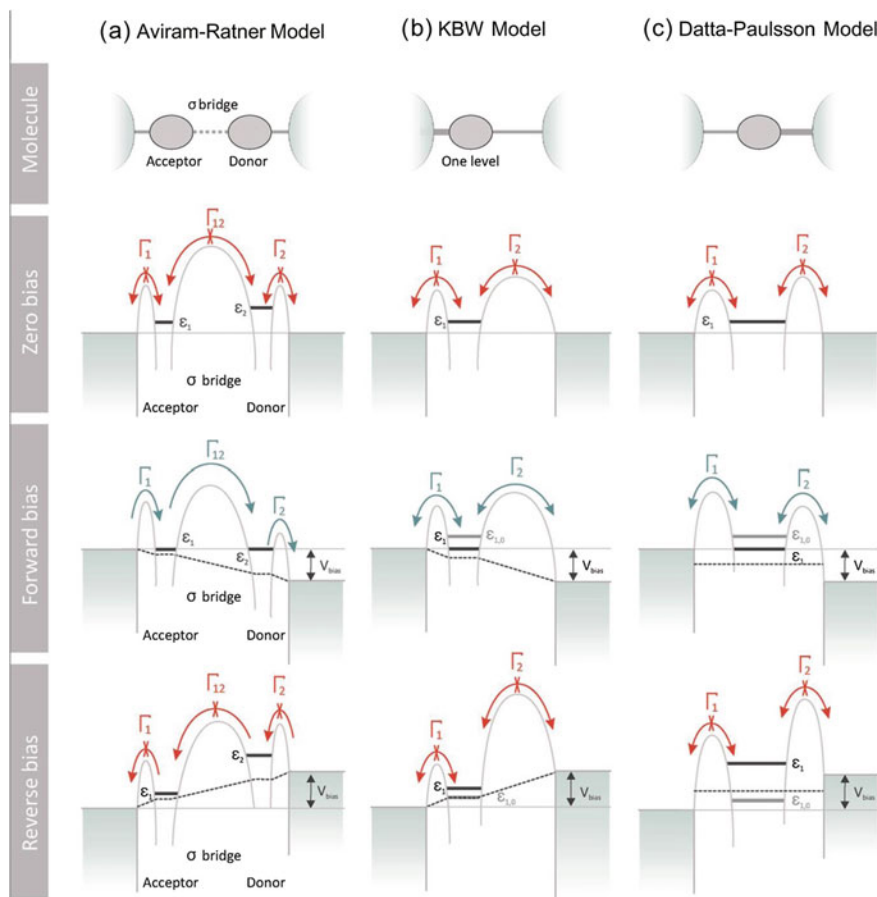


Fig. 9.3 Comparison of three models for molecular diodes (Γ_i represents the rates of tunneling steps). **a** Aviram–Ratner proposal with molecule levels shifting through the applied electric field. The subtle energy-level alignment for the donor and acceptor moieties, in combination with the large electrical spacer separating the two moieties, eventually leads to a difference in the current onset. **b** Simplified model, as proposed by Kornilovitch, Bratkovsky, and Williams (KBW), with one level. The level is shifted with respect to the applied electric field. **c** Considering the charging of the energy levels (proposed by Datta and Paulsson) can lead to diode behavior, even without level shifting by an electric field. Reprinted with permission from Ref. [14] Copyright 2012 American Chemical Society

AR Model [2]: According to this model, at a zero bias, the HOMO of the donor and the LUMO of the acceptor is slightly below and above the electrode's Fermi level, respectively. With application of positive bias, due to the alignment of the metal electrode's Fermi level with the lowest occupied molecular orbital (LUMO) of acceptor, the charge carriers are injected into acceptor from cathode, but charge cannot flow from acceptor to donor until the Fermi level of metal anode is lowered

enough so that charge can transfer from the highest occupied molecular orbital (HOMO) of donor to the metal electrode. In the reverse bias direction, charge transfer from metal electrode to acceptor will happen as the E_F of the metal electrode is lowered below the HOMO of acceptor. This will result electrons to tunnel from donor to acceptor through the barrier. The two separate energy levels ε_1 and ε_2 of the donor and acceptor, respectively, respond oppositely to the electric field resulting in energy-level alignment or misalignment responsible for the asymmetric charge transport. Essentially, according to AR model, rectification could be viewed as a different onset of resonant tunneling under forward and reverse bias directions.

KBW Model [12]: In this model, KBW applied AR mechanism to relatively simpler system with only one molecular orbital. According to this model, an essentially asymmetric tunneling barrier is responsible for rectification. Due to asymmetry in the molecule, the position of the orbital is not located symmetrically between the electrodes and most of the applied bias drops across longer insulating barrier. Hence, the conditions for resonant tunneling through the molecular levels are attained at different voltages under forward and reverse biases. Hence, alignment and misalignment of the molecular level with Fermi level of the electrodes depend on the bias directions leading to the rectification behavior. KBW model provides an important clue for choosing or designing simple molecules with asymmetry at one end or different length tails enacting different tunneling barriers compared to complex molecule required in the AR model, and it is proposed that the rectification ratio can be varied by changing the lengths of the insulating tails.

DP Model [13]: According to this model, it has been shown how the rectification can be achieved through asymmetric coupling of a symmetric molecule with the electrodes at the two ends. In this mechanism, the I - V characteristics are symmetric under low bias but become asymmetric under higher bias. Furthermore, under resonant conduction, this asymmetry results in conductance peak of different heights. According to this model, conduction through the molecule occurs through the same molecular level at opposite biases, and this is the main difference with AR and KBW models. Essentially, the induced asymmetry is due to the charging effect which is significantly high in single-molecular devices with tunneling barrier to the electrodes and the asymmetry in charging energies leads to the different tunneling rates between the molecular level and the two electrodes. Hence, the average population of the molecular level with two electrons depends on the direction of biases in the resonant tunneling condition, resulting rectification.

Experimentally, it is difficult to distinguish these three mechanisms from each other for several reasons. (1) It is difficult to chemically synthesize complex molecule required for Aviram-Ratner diode, and even it is more difficult to achieve a decoupling between donor and acceptor orbital in D- σ -A molecule. (2) It is difficult to control the coupling between the electrodes and the terminated groups of molecules due to several poorly understood interfacial interactions and random contact geometries. (3) As the molecular rectifier is mostly based on monolayer and not a single molecule, molecular dipole induces high and inhomogeneous electric

fields. (4) Compared to inorganic p-n junction diode, the operating electric field in molecular devices is at least one order of magnitude higher, so effect of high electric field on the electronic structure of molecules becomes extremely important.

9.4 Second Generation of Molecular Devices

The ultimate switching device with ON and OFF states capable of different logic operations would be based on single atom-based transistor, and such a device has been proposed by Wada et al. [15] with a switching speed of 1 THz. With present day technology, it has not been possible to achieve such ambitious device. However, similar device has been conceived using organic molecules. Stoddart and co-workers [16] have been able to demonstrate a molecular shuttle that could be switched electrostatically from one state to another using rotaxane molecule, as shown in Fig. 9.4. The rotaxane has two components, a molecular rod and a docking station based on benzidine and benzophenol, respectively. The rod has two beads based on two bulky triisopropylsilyl groups at the ends. When a proton source like trifluoro acetic acid (TFA) is added, the bead shifts toward biphenol station and can only be brought back by neutralizing the TFA with pyridine. This back and forth movement between two states can serve as controlled switch which has been configured to operate as XOR gate. Other active area of research is to conceive molecular switch based on bistable $I-V$ characteristics and $I-V$ characteristics with negative differential resistance (NDR). The molecular switch based on bistability and NDR has been envisaged as memory devices. Collier et al. [17] have demonstrated bistable $I-V$ characteristics in two terminal molecular devices based on catenane (Fig. 9.4) with amphiphilic phospholipid counter-ions sandwiched between an n -Si and Ti/Al electrodes. Repeatable read-write cycles have been demonstrated [16] using this bistable device. Reed and co-workers [18] have demonstrated NDR in a device based on molecule 2-amino-4,4-de(thynylphrnyl)-5-nitro-1-benzenethilate with nitroamine redox center sandwiched between two metal contacts in a nanopore. Strong NDR with a peak-to-valley ratio of $10^3:1$ has been observed (Fig. 9.5). No NDR was observed [18, 19] in control molecule (without nitro or amine moieties). Though the exact mechanism is not known yet, but phenomenologically, it has been explained [18, 19] as a two-step reduction. As bias increases, reduction of the molecule provides charge carriers, resulting increase in current which will continue to flow till the bias reaches to second reduction potential, and subsequently, the molecule is reduced to the dianion. Seminario et al. [20] have shown with ab initio calculations that current flows through the molecule only when the molecule is in reduced state because LUMO is only extended along the whole length of the molecule when it is in reduced state. But Ghosh et al. [21] have argued opposite, i.e., conduction happens resonantly with HOMO only when molecule is in oxidized state. The debate on the microscopic mechanism of NDR further fueled by another interesting work by Xue et al. [22] who have shown NDR in $I-V$ characteristics of single dibenzothiophenium 5-phenyl molecule by scanning

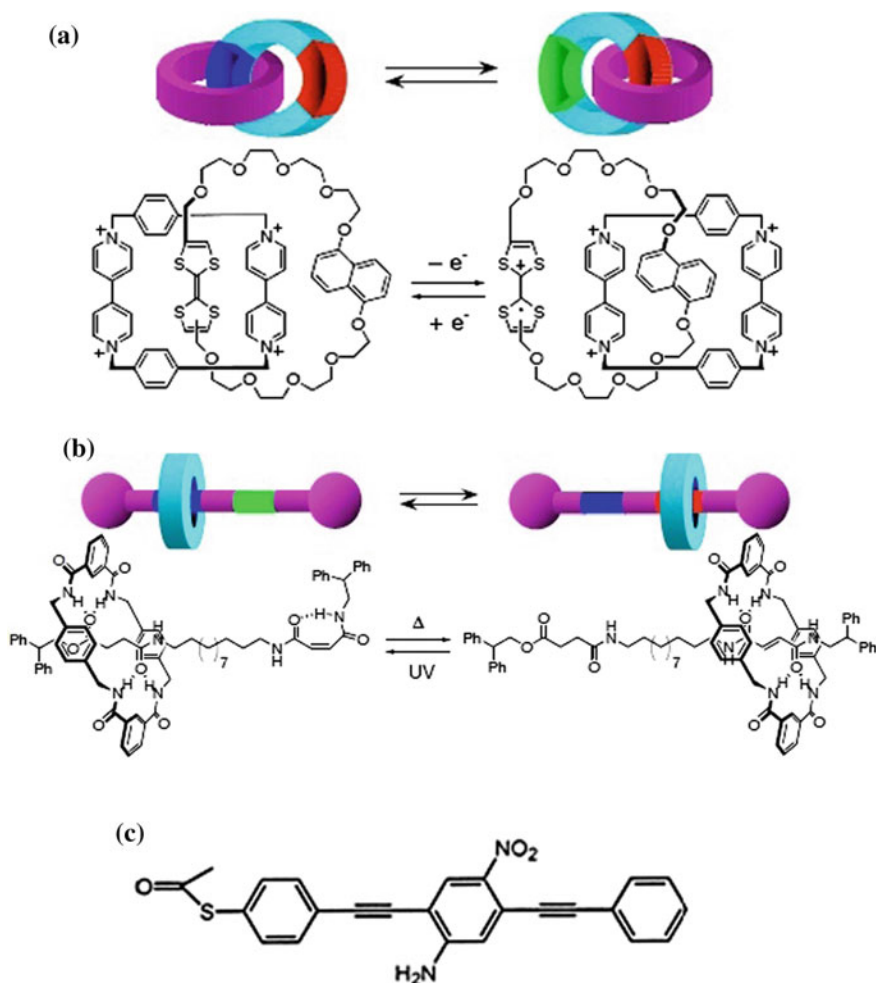


Fig. 9.4 **a** Schematic representation of two conformers of an electro active, bistable molecule catenane. **b** Schematic representation of a rotaxane which is a mechanically interlocked molecular architecture consisting of a dumbbell-shaped molecule threaded through a macrocycle. As the ends of dumbbell are larger than the diameter of the ring, rotaxane is trapped. **c** Molecule containing a nitroamine redox center [2-amino-4,4-de(thynyl)phnyl]-5-nitro-1-benzenethilate used in nanopore for two terminal-based devices [18, 19]

tunneling spectroscopy (STS). Interestingly, this molecule does not have nitroamine redox center, yet shows NDR. It has been argued [23] that reduced density of state at metal/molecule contact is prerequisite for observing NDR (Fig. 9.6). In case STS-based measurements, narrow tip of scanning tunneling microscope (STM) provides reduced density of state at tip/air/molecule contact, and since the other end of the molecule is attached to metallic substrate through a relatively

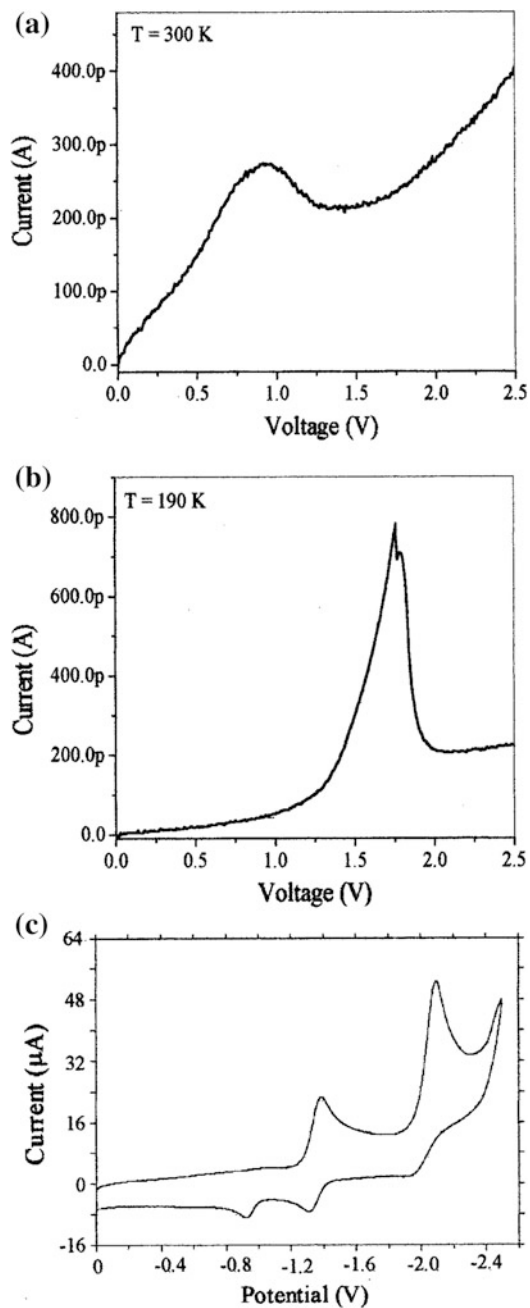


Fig. 9.5 $I-V$ characteristics of two terminal devices based on molecule containing a nitroamine redox center at **a** 300 K, **b** 190 K, **c** cyclic voltammogram of the molecule showing two reduction peaks. Reprinted with permission from Ref. [19] Copyright 2000 AIP Publishing LLC

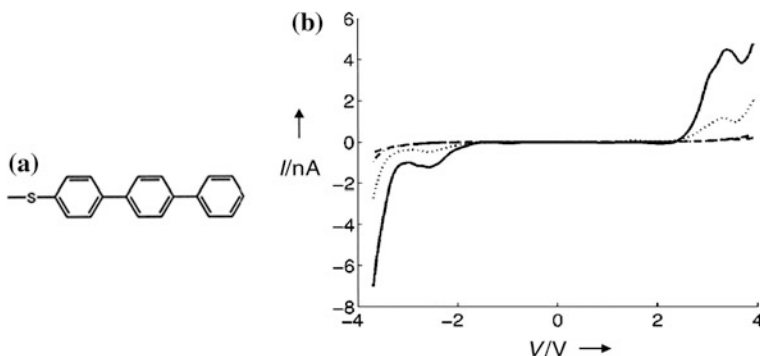


Fig. 9.6 **a** Molecule dibenzothiophenium 5-phenyl, **b** the I - V characteristics obtained by STS carried out on a monolayer of molecule. Reprinted with permission from Ref. [22] Copyright 1999, American Physical Society

strong thiol-gold covalent bond, the molecular orbital tends to align with the E_F of the substrate. When bias is applied, the molecular levels shift in one direction, while the tip density of states (DOS) shifts the other direction, and if the molecular levels cross the tip DOS, then one should observe NDR.

9.5 Third Generation of Molecular Devices

In third-generation molecular devices, mostly organic molecules are used as active device components and current transports through the molecules directly connected end-to-end with metal electrodes. Out of several platforms for third-generation molecular devices, single-molecule junctions based on a metal-molecule-metal architecture has received maximum attention. In addition to contemplated basic element for future molecular integrated circuit, the single-molecule junctions have immensely contributed to the fundamental understanding of mesoscopic transport by providing the most suitable platform for experimenting different predictions of quantum transport.

Efficient device fabrication based on single or few molecules requires development of suitable contact structure or pattern for characterization of molecular devices. It is difficult to study transport properties of single molecule by probing them between two symmetrical metal contacts due to lack of electrodes with separation in molecular dimension. There are two general approaches involving pre-formed contacts with nanometer separation between two electrodes. The first one is based on vertical device structures (VDS), where a self-assembled monolayer (SAM) of organic molecules is prepared on a metallic surface which is one contact and other contact is the tip of STM [24, 25] or conductive probe atomic force microscopy (AFM) [26], and crosswire techniques [27] belong to this class of structures in which two-crossed metallic wires separated by nanometer separation

hold the molecules vertically. These techniques are most suitable for few molecule-based devices; it is extremely difficult to employ these techniques for single molecule-based devices. The second one is based on lateral device structures (LDS), in which a pair of electrodes with nanometer separation is formed, and molecules are locked with their end groups within the gap using self-assembly technique. Such electrodes are fabricated on substrate using mechanically controlled break junction (MCEB) [28, 29], electromigration-induced break junction (EIBJ) [30–34] and electro-deposition [35–37]. In VDSs, the top contact to the molecule is made physically, whereas, only the bottom contact is chemically coupled to the molecule. It is difficult to avoid inbuilt asymmetry in VDSs due to different contact structures at the both end of the molecule. This poses great difficulty in distinguishing the cause of asymmetry in I - V characteristics as due to contact limited or due to asymmetry in the molecule. The devices based on LDSs can be fabricated in two different ways. In first approach, molecules are self-assembled on the metal surface before breaking and induced to migrate into the gap at low temperature. In this case, after breaking the break junctions, the residual interlink of metallic adhesion layer and the cantilever effect [38] of the suspended Au microelectrode cannot be ruled out. In the second approach [39–41], first a pair of electrode with nanometer-sized separation (nanogap) between them is created by an EIBJ technique performed at room temperature. There are several advantages of this method. The main advantage is that this method allows the break junction to be first characterized at room temperature, prior to deposition of molecules. A pair of electrodes with 1-2 nm separation can be realized with relatively high yield, as can be inferred from combined imaging and electrical characterization. This method allows the deposition of the desired molecule at the nanogap created at room temperature after initial characterization of the nanogap.

The first two methods, VDS based on scanning probe microscope (SPM) and LDS based on MCJB lack mechanical stability, as well as electrical stability required for transport measurements under different ambient conditions. It is even doubted [42] whether individual molecules are actually attached to the gap in break junctions fabricated by the methods proposed in Refs. 28, 29 and 43. In principle, our method of fabrication of two electrodes with nanometer separation is more or less similar to third method, [44, 45] except two main differences: (i) nanoelectrodes need not be fabricated at low temperature and (ii) nanoelectrodes can be fabricated without self-assembled molecules. Simplicity and reproducibility of our method stand it out of all the methods proposed or demonstrated for fabrication of nanoelectrodes. Moreover, though our method does not require sophisticated lithography, however is compatible with conventional processes for device fabrication. The fabrication of nanoelectrodes has been achieved by passing a large electrical current through a thin Au-finger with a notch at the middle, fabricated on SiO_2/Si substrates by photolithography. When high current passes through the Au-finger, electromigration driven breaking results two stable electrodes with nanometer separations, enabling transport measurements through nanometer size molecules. In order to form m - M - m junctions, organic molecules, such as 1,4 benzenedithiol (BDT), 1,4 benzenedimethanedithiol (BDMT), and thiolated ds-DNA

have been strongly bonded by self-assembly technique between two electrodes which are connected to suitable contact pads to facilitate further probing with different electrical characterization techniques or integration into with array of such devices.

In our method [39–41], 3000–5000 Å thermal oxide-coated silicon (Si) substrates were first silanized with a monolayer of 3-Mercaptopropyl trimethoxysilane (MPTMS). In silanization, the SiO₂ substrate was processed in four steps, (i) piranha clean, (ii) oxygen plasma, (iii) hydroxylation, and finally (iv) four hours of exposure to the MPTMS gaseous molecules inside a vacuum desiccators. The silanized SiO₂ samples were transferred immediately into the evaporation chamber for deposition of a 200–300 Å Au layer. The silane functional group of the MPTMS forms Si–O–Si covalent bonds with the SiO₂ surface silanols, leaving the –thiol group (–SH) of the molecule on the top leading to Au–S bond strong enough to hold the Au thin film tightly. A field emission scanning electron microscope (FESEM) image of the lithographically defined Au wire is shown in Fig. 9.7. For electrical characterization, each end of the Au micro wire is connected to a thick (~5000 Å) Au pad layer. The pressure was maintained at $2\text{--}3 \times 10^{-7}$ torr, during all depositions, and the deposition rate was maintained at 1 Å/s, monitored in situ using a quartz crystal thickness monitor. To localize the positions

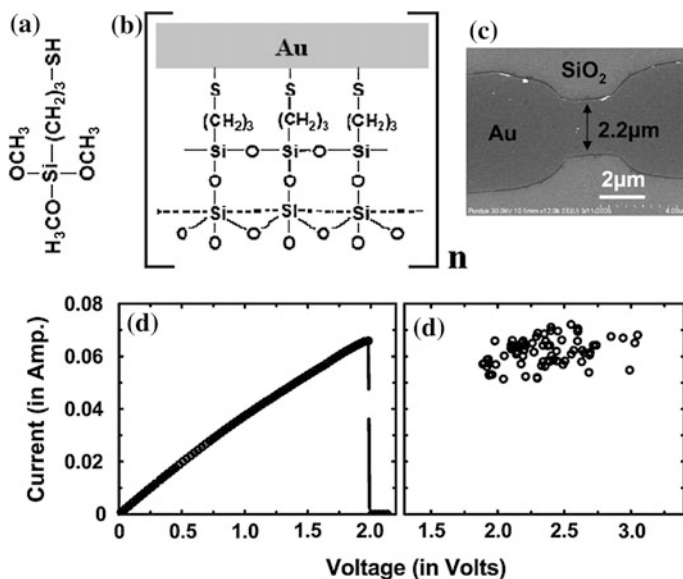


Fig. 9.7 **a** 3-Mercaptopropyl trimethoxysilane (MPTMS) molecule. **b** Schematic diagram of MPTMS monolayer adhesion that forms Si–O–Si covalent bonds with SiO₂ surface and Au–S bond with evaporated Au thin layers. **c** FESEM image of lithographically defined Au wire before electromigration. **d** I – V characteristics in Au wire during electromigration. **e** Threshold current and voltage at break point for some EIBJ devices. Reprinted with permission from Ref. [41] Copyright 2006, IEEE

of the nanogaps, lithographically Au-finger is notched at the middle (shown in Fig. 9.7). As voltage increases linearly across the Au-finger, at a threshold voltage V_{th} , current decreases abruptly by several orders of magnitude due to the formation of a gap which was subsequently imaged by FESEM. Initially, current through the wire increases linearly and after V_{th} Ohmic current changes to tunneling current through the nanogap created between two Au electrodes. The resistances of the Au wires, which were 30–50 $\mu\Omega$ before electromigration, change to M Ω –G Ω after the break. The break occurs when the driving voltage typically exceeds 1.5 V resulting in a nanogap due to the physical motion of Au atoms out of the high-current density areas, a phenomenon known as electromigration. The electromigration is the result of (i) the force due to the effect of electric field on the migrating ions and (ii) the wind force due to the scattering of the conduction electrons by the Au atoms. It has been observed that wires with longer notch width ($\sim 4 \mu\text{m}$) give a wider gap between the electrodes compared to that of shorter ones ($\sim 2 \mu\text{m}$). This can be explained by the threshold current density required for Joule heating for shorter width and longer width wires reaches at lower and higher bias, respectively. Higher bias makes the Au atoms move further apart with high field resulting in wider gap between the electrodes. Hence, electromigration is a combined effect of the maximum local Joule heating at the notch and the momentum transfer between the conduction electrons and diffusing metal ions.

Following electromigration, the nanogaps are characterized by FESEM. Figure 9.8 shows the FESEM image for two pairs of Au electrodes with sub-nm separation. The final gaps (the regions with shortest separation) were of length 1 nm over 5 nm width. Five chips, each having twenty five break junctions were examined under FESEM. The nanogaps with molecular dimension were mostly of 5–10 nm areas of the junctions separated by 1–5 nm and rest of the junctions showing gaps with 5–15 nm separation. The device yield is more than 20%, which is an improvement to the previously reported 10–15% device yield [46–48] using break junctions formed by electromigration. From FESEM imaging, it is difficult to estimate the exact gap length below 2 nm, but the separation of the subnanometer gap can be inferred from the conductivity measurement of nanogaps after the break. Figure 9.9 represents the histogram of the spectrum of conductance observed in nanogaps formed by EIBJ. The smallest separation has been observed to be located at one place along the whole width of the Au wire, and obviously, the observed conductivity can be attributed to the smallest gap region and cannot be affected by the other portions of the gap. We have observed at low bias the current through the smallest nanogaps is in the nanoampere to picoampere range, and the current through the gap more than 2 nm (as viewed through FESEM) is below the measurable limit of the picometer. As expected, current through the empty gap currents is in excellent agreement with the Fowler–Nordheim tunneling relation [49], as shown in Fig. 9.8. I – V characteristics of empty gap are reproducible in repeated scans ensuring the stability of the electrodes with nanogap with time and under high electric fields. It is extremely important that after the formation of gap, electrodes edges are not affected further due to application of high electric field. The length of

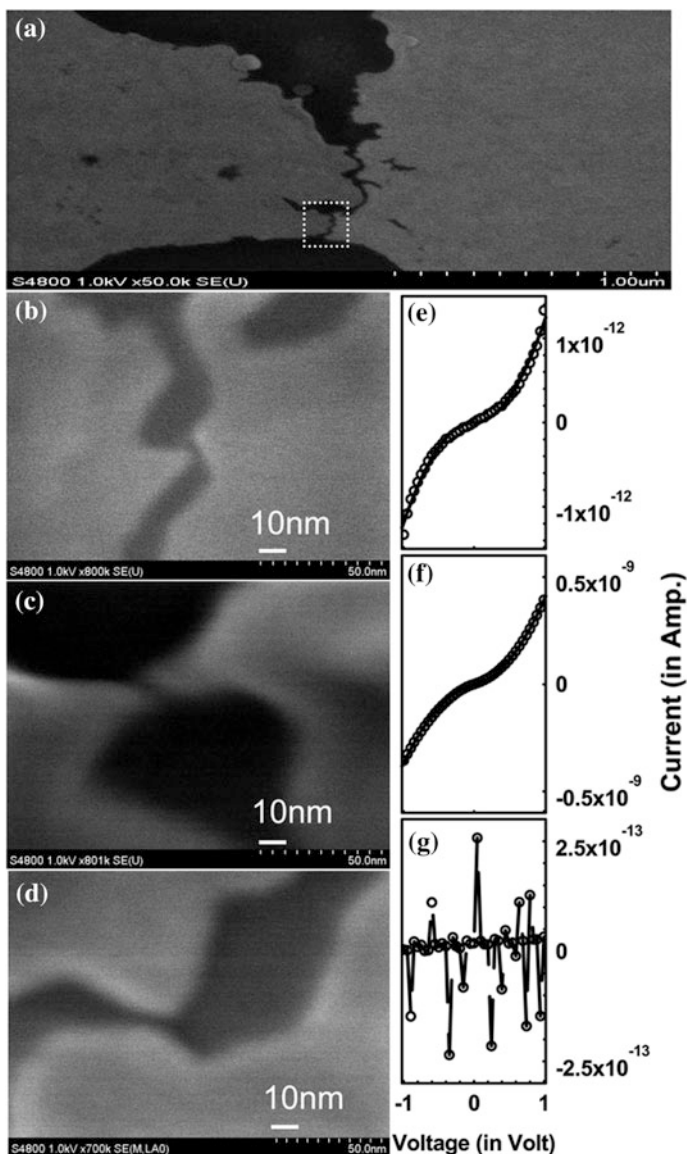
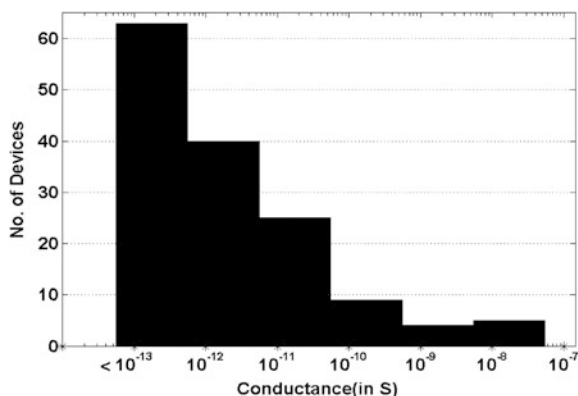


Fig. 9.8 FESEM images of EIBJ devices that show 1 nm gap created between two Au electrodes, **a** although Au wires are initially 2 μm wide, gap of length 1 nm and width 5 nm is observed **b** after break junction. Image (b) is zooming picture of selected portion in image (a). **e–g** Corresponds to empty gap I – V characteristics of EIBJ devices, respectively. *Solid lines* are Fowler–Nordheim fit to experimental data (*open circles*). Conductivity is measured (**e**), (**f**) for Au/empty gap/Au devices with gaps 2 nm, as confirmed through FESEM image (**b**) and (**c**). For devices with larger gap lengths (5 nm), conductivity falls below noise level of instrument (**g**). Reprinted with permission from Ref. [41] Copyright 2006, IEEE

Fig. 9.9 Histogram of conductances obtained from 150 nanogap in electromigration-induced break junction (Au/empty gap/Au) devices. Reprinted with permission from Ref. [41] Copyright 2006, IEEE



the gap is related to the tunneling conductance by the expression [50], $G_{\text{tun}} = \alpha \exp(-kd)$, where G_{tun} is the tunneling conductance, d is the gap length, and α and k are constants determined by the local structure. The tunneling conductance versus separation distance is reported [41] for Au–vacuum–Au structure comparable to these devices. This relationship can be described by values of $\alpha = 6.67 \times 10^{-8}$, and $k = 1.25 \times 10^{10} \text{ m}^{-1}$. From the tunneling conductance of the empty gaps, the separation of the nanogaps has been estimated [51]. As there is one order decrease in tunneling current in every 2 Å, the observed conductivity mostly is dominated by the separation localized at one point over the whole width.

9.5.1 Current Transport Through Single 1,4-Benzenedithiol (BDT) and 1,4-Benzenedimethanedithiol (BDMT) Molecules

Following the creation and subsequent characterization of the break junctions, 1 mM solutions of BDT or BDMT in dichloromethane or ethanol were used to deposit the desired molecules between the two electrodes separated with nanogap. This has been done either by immersing the whole chip in the solution or by putting a droplet on the chip. Whenever separation of the nanogap matches the length of BDT or BDMT molecules with thiol end groups, molecules dock between two electrodes and a stable chemical bond between the sulfur atom and Au surface is established. In order to verify the docking of molecular layers to Au surfaces, SAM using the same solution was grown on clean Au surfaces using the same immersion procedures and were subsequently characterized by reflection absorption infrared (RAIR) spectroscopy. RAIR spectra of BDT and BDMT are shown in the insets of Figs. 9.10 and 9.11 [39]. In case of BDT SAM, the peak at around 1500 cm^{-1} is due to stretch mode of C=C–C in benzene ring in BDT. The peaks at around 1000 cm^{-1} and 800 cm^{-1} are due to C–H in-plane and out-of-plane bends in

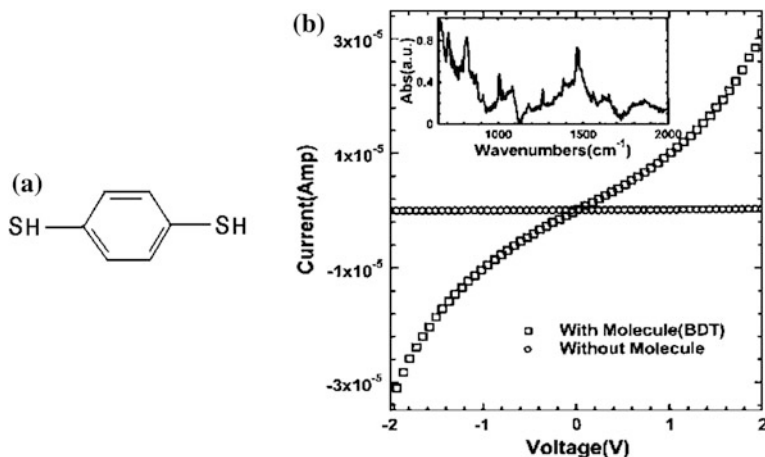


Fig. 9.10 **a** Benzene dithiol (BDT) molecule, **b** I - V characteristics of 1,4-benzene dithiol (BDT) at room temperature (*empty squares*), along with that of the nanogap before deposition of molecules (*empty circles*). Current through the break junction increases by more than two orders of magnitude after docking the BDT molecule. *Inset* shows the RAIR of BDT on Au. Reprinted with permission from Ref. [39] Copyright 2005 AIP Publishing LLC

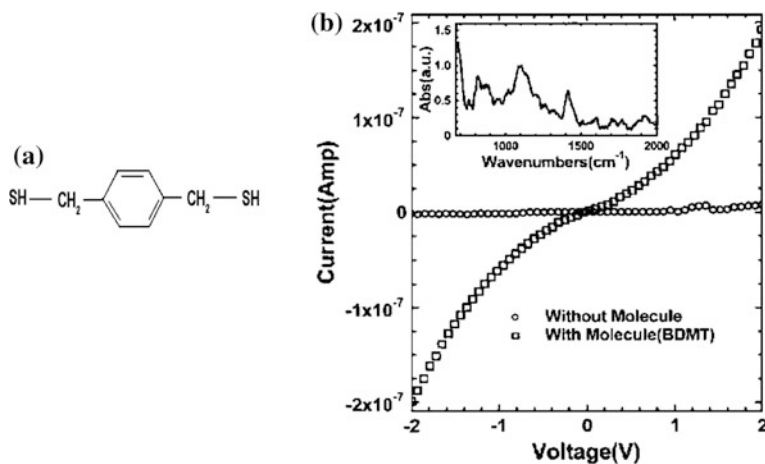


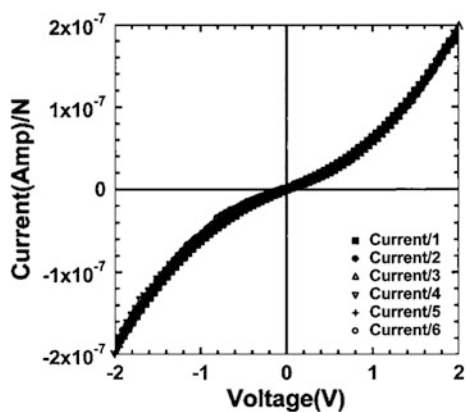
Fig. 9.11 **a** 1,4-benzenedimethanedithiol (BDMT) **b** I - V characteristics of BDMT at room temperature (*open squares*), along with that of the nanogap before deposition of molecules (*open circles*). Current through the break junction increases by more than two orders of magnitude after docking the BDMT molecule. *Inset* shows the RAIR of BDMT on Au. Reprinted with permission from Ref. [39] Copyright 2005 AIP Publishing LLC

BDT, respectively. The peaks in RAIR spectra of the BDMT SAM have similar origin as those in BDT.

Figures 9.10 and 9.11 show the I - V characteristics [39] for BDT and BDMT, respectively. The figures also show the I - V characteristics of the respective electrodes with nanogap before deposition of the molecules. I - V measurements were performed on more than 100 break junctions for each molecule. It has been observed that conductance increases with increasing deposition time of the molecules, and conductance of the nanogap electrodes increases for those structures for which the gap widths (inferred from pre-molecule conductance) were comparable to the molecular length, but there was no change in conductance with significantly larger gaps. Further, it should be pointed out here that the conductance did not systematically increase upon exposure to the only organic solvent, indicating that the observed conductance was not due to leakage paths along the oxide surface or solvent-induced reconfiguration of the contact structures. As expected, devices which show significant increase in conductivity following deposition of molecules generally exhibit similar I - V characteristics. Figure 9.12 shows that the I - V curves of six devices, each divided by an integer. When these curves are scaled by integers, they all collapse on one curve indicating that the curves observed for $N = 1$ must be due to single BDMT molecule. Similar characteristics have been observed by other groups [52–54] using SPM-based break junctions. Furthermore, I - V characteristics are shown in Fig. 9.10 correspond to a case in which a number of molecules can be considered to be conducted in parallel, while I - V characteristics shown in Fig. 9.11 correspond to the lowest observed conductance in this series, and most likely correspond to a single molecule.

Figures 9.10, 9.11 and 9.12 reveal several notable features of the I - V characteristics of the devices with BDT and BDMT molecules. (i) The I - V characteristics are linear at low bias (~ 0.3 V), and resistance near zero bias has been found to be 9 and 26 M Ω for single BDT and BDMT molecules, respectively. (ii) As expected due to the presence of the $-\text{CH}_2-$ groups at the two ends, the resistance of the single BDMT is higher than that of single BDT molecule. (iii) The low-field conductance is significantly higher than those observed in measurements using other contact structures, in particular using VDSs. (iv) The I - V characteristics

Fig. 9.12 Six representative I - V curves of BDMT from different groups, which are integer multiple of a fundamental curve. Curves are divided by 1, 2, 3, 4, 5, and 6. Reprinted with permission from Ref. [39] Copyright 2005 AIP Publishing LLC



over the whole range of bias are symmetric and nonlinear. (v) There is no conductance gap and this is consistent with the behavior expected from a molecule in which the density of states is broadened significantly due to strong coupling to the metallic electrodes at both ends of the molecule [55–58]. (vi) The superposition of all I - V traces on a curve for $N = 1$ (Fig. 9.14) provides evidence of stable Au-S contacts at both ends of the molecule and negligible in plane molecule-molecule interactions. In MCBJ, for current transport through a single molecule, contacts to the molecule are often made and broken by mechanically pulling apart the junction and then bringing the contacts back together between series of measurements. It has been suggested [51] that the current transport observed in early MCBJ structures may be through the overlapping pair of molecules bonded between two opposite facing electrodes, rather than through a single molecule attached to electrodes at both ends of the molecule. In the case of ECBJ-based devices, beyond a reasonable doubt, the Au-S bonds are stable at both ends of the molecule and the origin of symmetric and reproducible I - V characteristics may be different from those obtained using MCBJ.

9.5.2 Current Transport Through Single DNA

To investigate current transport through single DNA, three different 18-mer ds-DNA molecules were used for fabricating devices based on ECBJ. The molecules had thiol group attached to the 5' end through a $(\text{CH}_2)_6$ linker, for covalent attachment to the Au electrodes. The DNA sequences were chosen carefully so that they differ by their GC content and the corresponding melting temperatures. Three sequences are Seq-1: self-complementary SH-CGT ACA TGA TCA TGT ACG with GC content of 44.4%, Seq-2: SH-CAG TCA GGC AGT CAG TCA with GC content of 55.6% and Seq-3: self-complementary SH-CGT GCA CGT ACG TGC ACG with GC content of 66.7%. DNA disulfide groups were reduced and then purified, as described in Ref. [40]. The same sequences were also used without the thiol groups to serve as control. The purified DNA was subjected to annealing at 90 °C for 10 min in appropriate buffer. Subsequently, DNA was attached to Au by immersing the chips with array of ECBJ in 10 μM solution of thiolated ds-DNA.

I - V characteristics of the devices with DNA were obtained between -1V and $+1\text{V}$. Approximately, 15% of the devices showed an increase in current, attributed to the presence of covalently linked ds-DNA molecule in the nanogaps, whereas none of the control samples (DNA without thiol at ends) showed an increase in current. Figure 9.13 shows the I - V characteristics of two devices with sequences 1 and 3 which show about a three order increase in current when compared to the current in the control device. The devices were then subjected to a temperature ramp up to 400 K with a 30 s hold at 5 K increments, and then ramped back to room temperature. All the devices that were not exposed to any voltage stress during the temperature ramp, exhibited a reduction in current, when measured after the ramp, as shown in Fig. 9.13. It can be argued that the loss of conduction, which

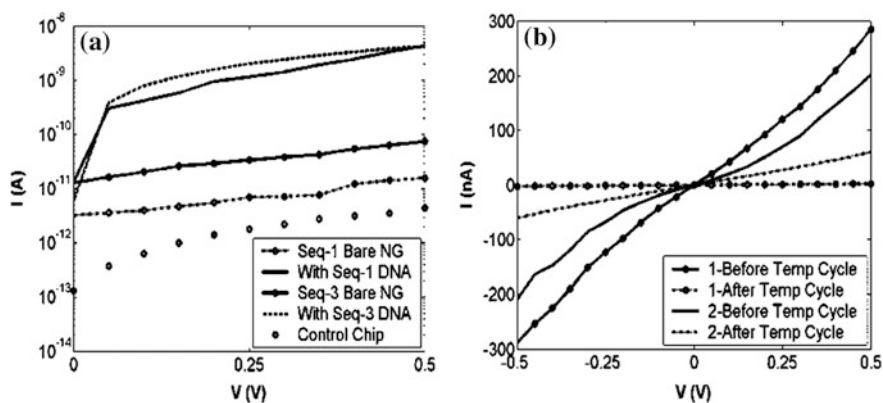
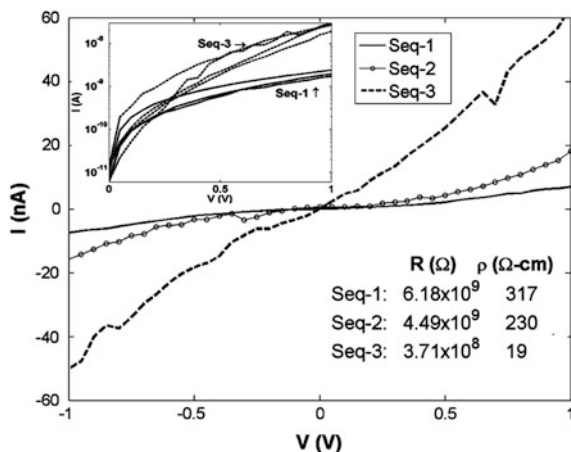


Fig. 9.13 **a** Comparison of current–voltage characteristics of conduction through bare nanogap, with DNA docked in sequence 1&3, and for the control chip after incubation in nonthiolated sequence 1, where no conduction was observed. **b** I – V plots for sequence 1 show decrease in conduction after temp cycling. Conduction was restored after reincubation and temp cycling. Reprinted with permission from Ref. [40] Copyright 2005 AIP Publishing LLC

was observed consistently with all different sequences, is due to the denaturing of DNA in the dry state. The melting of the DNA strands is facilitated due to the absence of significant number of counter-ions and water molecules and should occur within the 100 K temperature ramp subjected to the devices. The devices behave like electrical fuses which can be “blown” by a temperature ramp. There are two notable features observed in this set of experiments. (i) Firstly, at each temperature increment and stabilization during the ramp, I – V characteristics were measured and 50% of these devices did not show a decrease in current, as compared to about 20 devices which showed a decrease in current, after the temperature ramp. It can be argued that a voltage stress during the temperature ramp could reduce the denaturing of the molecule due to charging effects in the ds-DNA. (ii) Secondly, after the temperature ramp, the conduction in the devices with DNA was regained in about 10% devices when re-exposed to a buffer. It can be argued that it will be difficult to re-hybridize DNA strands in the absence of counter-ions and water molecules.

As there are three hydrogen bonds between G and C, conduction through G–C bridge would be higher compared to conduction through A and T which are bridged with two hydrogen bonds [59, 60], but this has not been demonstrated using electrical measurements in dry conditions. The DNA sequences were designed in such a way that in the linear dimension, no G and C bases were more than two bases away from each other. It has been found that resistance near zero bias for single DNA with three different sequences increases with decreasing GC content, as shown in Fig. 9.14. This can be explained by higher hopping efficiency of charge

Fig. 9.14 Current–voltage plots of the three DNA sequences. Close to 0 voltage, the resistance decreases with increasing GC content. The resistivity values assume a single molecule, 6.7 nm long and 2 nm in diameter. *Inset* shows a number of I – V plots for sequences 1 and 3, all measured on different devices. Reprinted with permission from Ref. [40] Copyright 2005 AIP Publishing LLC



carriers between G and C. As the ionization potential of G is the lowest ($G < A < C < T$), it is considered the easiest path for conduction of charge carriers [60] resulting less resistance to the charge flow in the sequence containing higher G–C pairs. This is responsible for the decrease in resistance between Seq-1 and Seq-3 by an order of magnitude. The resistance and resistivity obtained from the linear region of the I – V curves closer to zero bias are given in Fig. 9.14. Previously reported resistivity values are (i) 0.025Ω cm in DNA with diameter assumed to be 10 nm and length 1.7–2.9 μm , (ii) 1Ω cm for poly(dG)-poly(dC) with average resistance value for 50 nm of self-assembled DNA networks [61], (iii) 0.41Ω cm for h-DNA with diameter assumed to be 2 nm, and the conductivity was evaluated from the measured loss of sensitive resonant cavities operating at 100 GHz [58] and, (iv) $1 \text{ m}\Omega$ cm with assumed diameter of 2 nm and length of 600 nm [62]. Otsuka et al. have found resistance values from 109 to 106Ω with increasing relative humidity from 30 to 100% in 1 kb to over 35 kb long molecules, indicating the dependence of resistance on water molecules in the ambient [63]. The values are shown in Fig. 9.14, assuming one ds-DNA chain of 2 nm diameter and 6.72 nm length and could be lower limit on the resistivity, as there can be more than one DNA molecules bridging the gap.

In summary, it has been shown that ECJB-based method to form electrodes with nanometer scale spacing to dock single or few molecules between the electrodes is the most efficient and reliable method to fabricate the most fundamental device for molecular electronics. The measured I – V characteristics of two short organic molecules and relatively long molecule such as DNA show repeatable characteristics. The absence of conductance gap and the relatively large conductance values at low bias indicate the strong coupling between molecules and electrodes. This method can be used effectively to investigate electrical transport through a large number of important organic molecules. Moreover, it has been shown that the denaturing of DNA can be studied electrically and ds-DNA molecule can be used as a fuse that can “blow” at higher temperature reversibly. In addition, it has been

shown how the resistance of DNA depends on sequence. These findings have potential to be a first toward DNA-based molecular electronics and direct label-free detection of DNA hybridization.

9.6 Theoretical Aspect for Conduction Through Single Molecule

The conductance of single molecules is a complex issue because it not only depends on electronic structure of molecule, but also depends on the coupling of individual molecule with macroscopic contacting pads. If the conduction through single or bunch of molecules is treated as mesoscopic conductor, then conductance is proportional to the transmission probability of electron from left electrode (L) to right electrode (R), between which the molecule is attached and can be expressed as

$$G = \frac{2e^2}{h} T$$

where e is the electron charge, h is the Planck's constant, and T is the total transmission probability over all transmission channels between L and R. If $T = 1$, i.e., when there is no molecule between L and R, G is $2e^2/h$ which is 77481 nS, equivalent to 12.9 K Ω . Hence, resistance of single molecule cannot be less than 12.8 K Ω . T which strongly depends on the coupling strength between molecule and electrode and can be given by

$$T = T_R T_L T_{\text{mol}}$$

where T_R , T_L , and T_{mol} are the transmission coefficient of the left interface, right interface, and molecule, respectively, and G can be given by

$$G = \frac{2e^2}{h} T_R T_L T_{\text{mol}}$$

The total current I from the left electrode L to the right electrode R, due to the presence of either one or many molecules in the gap, is given by

$$I = \frac{2e}{h} \int_{-\infty}^{\infty} [f_L(E) - f_R(E)] \text{Tr} \{ G^a(E) \Gamma^R(E) G^r(E) \Gamma^L(E) \} dE$$

where $\text{Tr}\{\}$ is the trace operator, $G_a(E)$ and $G_r(E)$ are the advanced and retarded Green's function for the molecule, respectively, and $\Gamma^R(E)$ and $\Gamma^L(E)$ are the matrices representing the coupling between molecule and right and left electrodes, respectively. This formalism also depends on the alignment of the molecular energy

levels, i.e., HOMO and LUMO, relative to the Fermi levels of the metal electrode. The coupling strength between the electrons in the molecules and those in the electrodes is the most important aspect of nonequilibrium Green function formalism for molecular transport [7]. There are three coupling regimes based on the relative strength of coupling (Γ) and the single-electron charging energy U which is the energy required to add or remove an electron to the molecule or from the molecule, respectively. These regimes are classified as (i) weak coupling ($\Gamma \ll U$), (ii) strong coupling ($\Gamma \gg U$), and (iii) intermediate coupling ($(\Gamma \sim U) \sim U$). Essentially, these three different coupling regimes indicate different degrees of overlap of the wave functions of the molecules and that of metal electrodes, resulting in different transport mechanisms, schematically shown in Fig. 9.15 [64]. In the weak coupling regime, an whole electron transfers from molecule to electrode or vice versa, so that the electron transport happens through a two-step process in which the electrons first hop from one electrode to the molecule, which has matching energy levels, and then hop to other electrode (Fig. 9.15a). In the absence of matching energy level, charge transport will be blocked unless an appropriate bias voltage high enough is applied so that it can overcome e-e repulsion, i.e., U to bring the Fermi energy of the electrode to the molecular energy levels. This phenomenon is also known as the Coulomb blockade. In the intermediate coupling regime, due to moderate interaction with electrode, molecular energy levels broaden and the injected electron from the electrode will be affected by the electrons on the molecule (Fig. 9.15b). In a

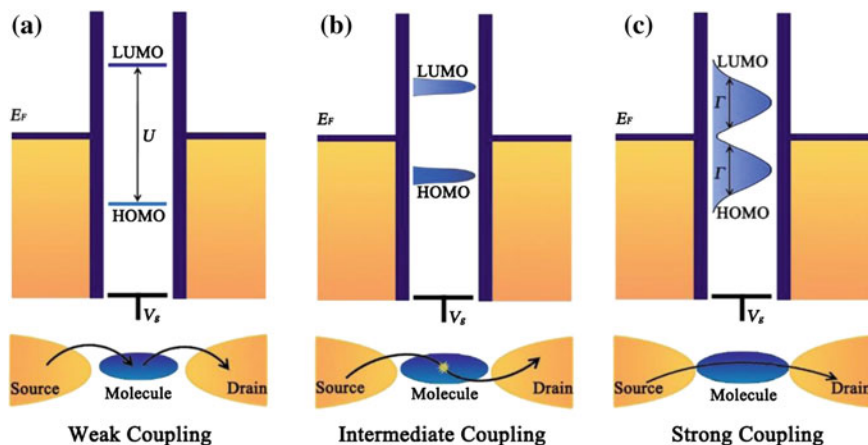


Fig. 9.15 Schematic representation of the energy levels and the charge transport processes of the molecular junctions with different coupling strengths between the molecules and the electrodes. **a** In the weak coupling regime ($\Gamma \ll U$), the HOMO and the LUMO of the molecules are well defined, and the electron transport occurs in a two-step process. **b** In the intermediate coupling regime ($\Gamma \sim U$), the HOMO and the LUMO become broader and closer to the Fermi energy of electrodes (E_F), and the electron transport occurs through the molecules interacting with the electrons on the molecules. **c** In the strong coupling regime ($\Gamma \gg U$), a large broadening of the molecular energy levels occurs, and electrons move from the source to the drain through a one-step process. Reprinted with permission from Ref. [64] Copyright 2013 Royal Society of Chemistry

situation, when there is an unpaired electron on the molecule, its spin state can be reversed by electrons injected from the electrode leading to a spin screening that could result in different transport phenomena. A zero-bias Kondo resonance is the result of such spin screening. Other possibility is a simultaneously tunneling process, in which one electron tunnels into the LUMO of the molecule with another electron simultaneously tunneling out of the HOMO, leaving the molecule in the excited state. In the strong coupling regime, the energy levels of the molecules are considerably broadened due to substantial overlapping of the molecule–electrode electronic states enabling partial, i.e., fractional charge transfer between the molecules and the electrodes (Fig. 9.15c). Therefore, the electron could virtually transport from one electrode to another through a one-step coherent process without stopping on the molecules. The absence of Coulomb blockade and observation of symmetric I – V characteristics further support strongly coupled regime. In this case, the conductance gap $E_{\text{gap}} \sim |E_F - \varepsilon_0|$ will be reduced by the contact and thermal broadening as shown in Fig. 9.15 given by Damle et al. [56] $E_{\text{gap}} \sim [(E_F - \varepsilon_0) - (2\Gamma - 4k_B T)]$, where ε_0 is the molecular level. The strong broadening of molecular levels due to covalent bonding at both contacts and a large charging energy can account for the observed reduction of the conductance gap.

9.7 Outlook and Open Questions

To take molecular electronics further so that several single molecule-based devices demonstrated as *proof-of-concept* can be practical devices, the combination of the recently developed techniques and traditional micro-fabrication techniques perfected over the decades for Si-industry is the need of the hour. For example, gating of two terminal break junction-based single molecular device is required to achieve functionalities for ultimate molecular circuit. Further, application of novel materials, for example, fabrication of single-molecule devices using graphene electrodes separated with a variable gap will take molecular electronics to next level. However, there remains several open questions in the different aspects of molecular electronics. Though there seems to exist a consensus on transport mechanism through single molecule, but several major issues such as, (i) the relationship between the molecular structure and intra molecule quantum interference, (ii) intermolecular interactions and their effect on charge transport, (iii) exact role of electrodes on the conductance quantization of single molecule, (iv) charge transport in single molecule to multimolecule junctions, (v) transport in intermediate regime where charging energy is close to level broadening and (vi) the spin-related effect such as Kondo effect and other many body effects remain as open questions and require further experimental and theoretical investigations. Though, ultimate limit for electronic device minimization will depend on the control of device with atomic accuracy, but it is generally accepted that realistically only the molecules can provide such control in subnanometer regime. It should be emphasized that there is no reason to believe that molecular electronics will replace robust Si-based

microelectronics, but it has potential to complement Si-based technology by providing molecule-based nanodevices with novel functionalities which at present is beyond the scope of conventional solid-state devices. The experimental and theoretical research on molecular electronics in last two decades exhibited significant scientific achievement which has brought scientists and engineers from different disciplines together. But, it is worth mentioning that over hype and unrealistic enthusiasm for rapid exploration of molecular electronics may not be compatible with systematic exploration practiced with great success in microelectronics industry.

References

1. G.E. Moore, *Electronics* **38**, 114–117 (1965)
2. A. Aviram, M.A. Ratner, *Chem. Phys. Lett.* **29**, 277–283 (1974)
3. R.M. Metzger, B. Chen, U. Höpfner, M.V. Lakshmikantham, D. Vuillaume, T. Kawai, X.L. Wu, H. Tachibana, T.V. Hughes, H. Sakurai, J.W. Baldwin, C. Hosch, M.P. Cava, L. Brehmer, G.J. Ashwell, *J. Am. Chem. Soc.* **119**, 10455–10466 (1997)
4. Dong Xiang, Xiaolong Wang, Chuancheng Jia, Takhee Lee, Xuefeng Guo, *Chem. Rev.* **116**, 4318–4440 (2016)
5. R. Lloyd Carroll, C.B. Gorman, *Angew. Chem. Int. Ed.* **41**, 4378–4400 (2002)
6. D. Xiang, X. Wang, C. Jia, T. Lee, X. Guo, *Chem. Rev.* **116**, 4318–4440 (2016)
7. R.M. Metzger, *Chem. Rev.* **115**, 5056–5115 (2015)
8. Z. Wei, M. Kondratenko, Lê H. Dao, D.F. Perepichka, *J. Am. Chem. Soc.* **128**, 3134–3135 (2006)
9. C. Krzeminski, C. Delerue, G. Allan, D. Vuillaume, R.M. Metzger, *Phys. Rev. B* **64**, 085405–085410 (2001)
10. S. Datta, W. Tian, S. Hong, R. Reifenberger, J.I. Henderson, C.P. Kubiak, *Phys. Rev. Lett.* **79**, 2530–2533 (1997)
11. M. Elbing, R. Ochs, M. Koentopp, M. Fischer, C. von Hänisch, F. Weigend, F. Evers, H.B. Weber, M. I Mayor, *PNAS* **102**, 8815–8820 (2005)
12. P.E. Kornilovitch, A.M. Bratkovsky, R.S. Williams, *Phys. Rev. B* **66**, 165436–165446 (2002)
13. F. Zahid, A.W. Ghosh, M. Paulsson, E. Polizzi, S. Datta, *Phys. Rev. B* **70**, 245317–245321 (2004)
14. E. Lörtscher, B. Gotsmann, Y. Lee, L. Yu, C. Rettner, H. Riel, *ACS Nano* **6**, 4931–4939 (2012)
15. Y. Wada, T. Uda, M. Lutwyche, S. Kondo, S. Heike, *J. Appl. Phys.* **74**, 7321–7328 (1993)
16. R.A. Bissell, E. Cordova, A.E. Kaifer, J.F. Stoddart, *Nature* **369**, 133–137 (1994)
17. C.P. Collier, G. Mattersteig, E.W. Wong, Y. Luo, K. Beverly, J. Sampaio, F.M. Raymo, J.F. Stoddart, J.R. Heath, *Science* **289**, 1172–1175 (2000)
18. J. Chen, M.A. Reed, A.M. Rawlett, J.M. Tour, *Science* **286**, 1550–1552 (1999)
19. J. Chen, W. Wang, M.A. Reed, A.M. Rawlett, D.W. Price, J.M. Tour, *Appl. Phys. Lett.* **70**, 1224–1226 (2000)
20. J.M. Seminario, A.G. Zacarias, J.M. Tour, *J. Am. Chem. Soc.* **122**, 3015–3020 (2000)
21. A.W. Ghosh, F. Zahid, S. Datta, R.R. Birge, *Chem. Phys.* **281**, 225–230 (2002)
22. Y.Q. Xue, S. Datta, S. Hong, R. Reifenberger, J.I. Henderson, C.P. Kubiak, *Phys. Rev. B* **59**, R7852–R7855 (1999)
23. Y. Karzazi, J. Cornil, J.L. Bre.das, *J. Am. Chem. Soc.* **123**, 10076–10084 (2001)
24. S. Datta, W. Tian, S. Hong, R. Reifenberger, J.I. Henderson, C.P. Kubiak, *Phys. Rev. Lett.* **79**, 2530–2533 (1997)

25. E.G. Emberly, G. Kirzenow, *Phys. Rev. Lett.* **91**, 188301–188304 (2003)
26. D.J. Wold, C.D. Frisbie, *J. Am. Chem. Soc.* **123**, 5549–5556 (2001)
27. J.G. Kushmerick, D.B. Holt, J.C. Yang, J. Naciri, M.H. Moore, R. Shashidhar, *Phys. Rev. Lett.* **89**, 086802–086804 (2002)
28. M.A. Reed, C. Zhou, C.J. Muller, T.P. Burgin, J.M. Tour, *Science* **278**, 252–254 (1997)
29. C. Kergueris, J.P. Bourgoin, S. Palacin, D. Esteve, C. Urbina, M. Magoga, C. Joachim, *Phys. Rev. B* **59**, 12505–12513 (1999)
30. W. Linag, M.P. Shores, M. Bockrath, J.R. Long, H. Park, *Nature* **417**, 725–729 (2002)
31. J. Park, A.N. Pasupathy, J.I. Goldsmith, C. Chang, Y. Yaish, J.R. Petta, M. Rinkoski, J. P. Sethna, H.D. Abruña, P.L. McEuen, D.C. Ralph, *Nature* **417**, 722–725 (2002)
32. L.H. Yu, D. Natelson, *Nano Lett.* **4**, 79–83 (2004)
33. K.I. Bolotin, F. Kuemmeth, A.N. Pasupathy, D.C. Ralph, *Appl. Phys. Lett.* **84**, 3154–3156 (2004)
34. H. Park, A.K.L. Lim, A.P. Alivisatos, J. Park, P.L. McEuen, *Appl. Phys. Lett.* **75**, 301–303 (1999)
35. F. Morpurgo, C.M. Marcus, D.B. Robinson, *Appl. Phys. Lett.* **74**, 2084–2086 (1999)
36. Z. Li, H.X. He, N.J. Tao, *Appl. Phys. Lett.* **77**, 3995–3997 (2000)
37. M.M. Deshmukh, A.L. Prieto, Q. Gu, H. Park, *Nano Lett.* **3**, 1383–1385 (2003)
38. T.B. Gabrielson, I.E.E.E. *Trans. Electron. Devices* **40**, 903–909 (1993)
39. S. Ghosh, H. Halimun, A.K. Mahapatro, J. Choi, S. Lodha, D. Janes, *Appl. Phys. Lett.* **87**, 233509-3 (2005)
40. S.M. Iqbal, G. Balasundaram, S. Ghosh, D.E. Bergstrom, R. Bashir, *Appl. Physics Lett.* **86**, 153901–153903 (2005)
41. A.K. Mahapatro, S. Ghosh, D.B. Janes, I.E.E.E. *Tran, NANO* **5**, 232–237 (2006)
42. E.G. Emberley, G. Kirzenow, *Phys. Rev. B* **64**, 235412–235419 (2001)
43. J. Reichert, R. Ochs, D. Beckmann, H.B. Weber, M. Mayor, H.V. Löhneysen, *Phys. Rev. Lett.* **88**, 176804–176807 (2002)
44. H. Park, A.K.L. Lim, A.P. Alivisatos, J. Park, P.L. McEuen, *Appl. Phys. Lett.* **75**, 301–304 (1999)
45. J. Park et al., *Nature (London)* **417**, 722–725 (2002)
46. W. Linag, M.P. Shores, M. Bockrath, J.R. Long, H. Park, *Nature* **417**, 725–729 (2002)
47. J. Park et al., *Nature* **417**, 722–725 (2002)
48. H. Park, A.K.L. Lim, A.P. Alivisatos, J. Park, P.L. McEuen, *Appl. Phys. Lett.* **75**, 301–303 (1999)
49. S.M. Sze, *Physics of Semiconductor Devices* (Wiley, New York, 1969)
50. C.Z. Li, H.X. He, N.J. Tao, *Appl. Phys. Lett.* **77**, 3995–3997 (2000)
51. C. Kergueris, J.P. Bourgoin, S. Palacin, D. Esteve, C. Urbina, M. Magoga, C. Joachim, *Phys. Rev. B* **59**, 12505–12513 (1999)
52. B. Xu, N.J. Tao, *Science* **301**, 1221–1223 (2003)
53. X. Xiao, B. Xu, N.J. Tao, *Nano Lett.* **4**, 267–271 (2004)
54. X.D. Cui et al., *Science* **294**, 571–574 (2001)
55. W. Tian et al., *J. Chem. Phys.* **109**, 2874–2882 (1998)
56. P.S. Damle, A.W. Ghosh, S. Datta, *Chem. Phys.* **281**, 171–187 (2002)
57. P.S. Damle, A.W. Ghosh, S. Datta, *Phys. Rev. B* **64**, 201403–201406 (2001)
58. K.-H. Yoo, D.H. Ha, J.-O. Lee, J.W. Park, J. Kim, J.J. Kim, H.-Y. Lee, T. Kawai, H.Y. Choi, *Phys. Rev. Lett.* **87**, 198102–198105 (2001)
59. Ch. Adessi, S. Walch, M.P. Anantram, *Phys. Rev. B* **67**, 081405–081408 (2003)
60. M. Di Ventra, M. Zwolak, in *DNA Electronics in Encyclopedia of Nanoscience and Nanotechnology*, ed. by H.S. Nalwas (American Scientific Publishers, California, 2004)
61. Lintao Cai, Hitoshi Tabata, Tomoji Kawai, *Appl. Phys. Lett.* **77**, 3105–3106 (2000)
62. H.W. Fink, C. Schönberger, *Nature* **398**, 407–410 (1999)
63. Y. Otsuka, H. Lee, J. Gu, J. Lee, K.-H. Yoo, H. Tanaka, H. Tabata, T. Kawai, *Jpn. J. Appl. Phys.* **41**, 891–894 (2002)
64. C. Jiaa, X. Guo, *Chem. Soc. Rev.* **42**, 5642–5660 (2013)